Received: 20 January 2026 | Revised: 15 July 2026 | Accepted: 27 July 2026 | Published online: 14 August 2026

REVIEW

Smart Wearable Technology
2026, Vol. 00(00) 1–10
DOI: 10.47852/bonviewSWT62029149

BON VIEW PUBLISHING

# The Role of Material Parameters in the Buckling Behavior of Stiff/Soft Bilayer Films

**Hui He[1,#], Yufeng Chen[2,#], Xintong Shen[2,#], Feng Chen[2], Zhixiang Wang[2] and Yancheng Meng[2,*]**

[1] *Nanjing Medical University, China*

[2] *MIIT Key Laboratory of Aerospace Information Materials and Physics, College of Physics, Nanjing University of Aeronautics and Astronautics, China*

**Abstract:** A stiff/soft bilayer film is prone to losing surface stability under compression, resulting in various buckling patterns, including wrinkles and period-doubling folds. This phenomenon has attracted considerable attention over the past two decades owing to its potential applications in flexible electronics, strain control, and thin-film property tuning. However, theoretically studying the post-buckling behavior beyond period-doubling folds is a major challenge due to strong nonlinearity, highlighting the need for new models based on alternative approaches. This study clarifies how material parameters control the buckling and post-buckling behavior of stiff/soft bilayer films, with particular emphasis on the thickness ratio, modulus ratio, Poisson's ratio, and the scaling law for higher-order instability. Rather than treating applied compression as the primary determinant of pattern evolution, we identify the intrinsic geometric and elastic parameters of the bilayer as the main controlling factors. The thickness ratio is highlighted as the dominant geometric parameter governing the onset of local wrinkling, the suppression or delay of secondary period-doubling instability, and the transition between local and global buckling. The modulus ratio and Poisson's ratio further tune the critical wavelength and critical strain through the effective plane-strain modulus contrast and, together with the thickness ratio, define the equivalent thickness ratio used in the scaling description of the post-buckling instabilities.

**Keywords:** buckling behavior, bilayer films, material parameters

## 1. Introduction

Buckling is prevalent in organisms, engineering structures, and celestial shells. In particular, buckling behavior is commonly observed in stiff/soft bilayer systems. When a stiff membrane meets a soft film, the bilayers always tend to lose their stability under compression [1, 2] and exhibit various morphological instability modes [3–10], that is, buckling patterns. The primary instability mode is characterized by regular wrinkles [11–16], particularly evident at a high stiff-to-soft modulus ratio. These wrinkles maintain a uniform surface perimeter during evolution, corresponding to the critical wavelength $\lambda_0$ at the onset of wrinkling instability. $\lambda_0$ can be regarded as a characteristic length of buckling deformation, providing a key reference for quantifying advanced buckling modes. Meng et al. provide its universal expression [17]. This expression takes on simpler forms in limiting cases. For example, when the soft film thickness approaches infinity, the $\lambda_0$ expression reduces to Eq. 1, denoted as $\lambda_{0\text{-upper}}$

$$\lambda_{0-\text{upper}} = At_{\text{m}}, A = \pi\left(\frac{2}{3}\frac{\overline{E}_{\text{m}}}{\overline{E}_{\text{s}}}\right)^{1/3}\left[\frac{3-4\mu_{\text{s}}}{(1-\mu_{\text{s}})^2}\right]^{1/3} \tag{1}$$

***Corresponding author:** Yancheng Meng, MIIT Key Laboratory of Aerospace Information Materials and Physics, College of Physics, Nanjing University of Aeronautics and Astronautics, China. Email: yanchengmeng@nuaa.edu.cn
**#Co-first author**

where $\overline{E_{\text{i}}} = E_{\text{i}}/(1\text{-}\mu_{\text{i}}^2)$ with $i$ = m or s, where m and s correspond to the stiff membrane and soft film, respectively. $E_{\text{m}}$ and $\mu_{\text{m}}$ are Young's modulus and Poisson's ratio of the stiff membrane, respectively, while $E_{\text{s}}$ and $\mu_{\text{s}}$ are those of the soft film; $t_{\text{m}}$ refers to the thickness of the stiff membrane. Meanwhile, when the thickness ratio of the soft film to the stiff membrane approaches 1, there is another approximate form ($\lambda_{0\text{-lower}}$) of the $\lambda_0$ expression, that is,

$$\lambda_{0-\text{upper}} = At_{\text{m}}, A = \pi\left(\frac{2}{3}\frac{\overline{E}_{\text{m}}}{\overline{E}_{\text{s}}}\right)^{1/3}\left[\frac{3-4\mu_{\text{s}}}{(1-\mu_{\text{s}})^2}\right]^{1/3} \tag{2}$$

where $t_{\text{s}}$ is the thickness of the soft film.

Upon further compression, the next instability mode occurs in period-wrinkled membranes [3, 18–23], manifested mainly as wrinkle-to-fold transitions driven by stress localization [3, 22, 24–26]. For details, a period-doubling fold occurs when the initially uniform wrinkle pattern can no longer distribute the imposed compression evenly [22, 24, 25]. The deformation then localizes into every other wrinkle valley, so that alternate valleys grow deeper while neighboring wrinkles become relatively weaker [22]. This localization is governed by the elastic constraint of the soft film: when the film can deform inward more easily than outward, concentrating deformation in selected valleys becomes energetically favorable. This transition results in double and quadruple period folds in a stiff membrane on a sufficiently thick soft film for energy minimization. Thus, period-doubling is not merely a geometric change in wavelength but a lower-energy post-buckling state selected by the bilayer to reduce the combined bending energy of the stiff membrane and deformation energy of the soft film [24].

In essence, there is a recognized progression of the buckling evolution in the stiff/soft bilayers. Specifically, a stiff membrane on a deep soft film will lose its stability, forming wrinkles (first-order instability with the period of $\lambda_0$) when the strain exceeds its primary critical value $\varepsilon_0$. Subsequently, a period-doubling fold (developed from two primary wrinkles, second-order instability with a period of $2\lambda_0$) occurs as the strain exceeds the critical value $\varepsilon_1$. Finally, period-quadrupling folds or creases (developed from two period-doubling folds, with an instability period of $4\lambda_0$) occur when the strain exceeds $\varepsilon_2$. Both theoretical analyses and previous experiments have suggested that this established route governs the buckling evolution when the stiff-to-soft modulus ratio is sufficiently high [27, 28].

However, the most recent experimental results have shown that the buckling evolution in silicon oxide ($SiO_{1.8}$)/polydimethylsiloxane (PDMS) bilayer films with a modulus ratio larger than 10000 does not strictly follow the route discussed above [9, 29]. In detail, when the ratio of the soft film thickness ($t_s$) to stiff membrane thickness ($t_m$) is below 200, the buckling evolution will be blocked in the first-order instability. Consequently, only single-period ($\lambda_0$) wrinkles, folds, and creases emerge. Meanwhile, when the thickness ratio is larger than 200, second-order instability appears, where the buckling behavior begins with wrinkles (first order) and ends with a period-doubling fold (second order). Period-quadrupling bifurcation (fourth order) does not occur until the thickness ratio surpasses 750, which corresponds to the recognized buckling evolution route from wrinkles to period-doubling folds to period-quadrupling folds. In addition, a series of studies confirmed that the stiff-to-soft modulus ratio also influences buckling evolution [27, 30]. These experimental findings indicate that the buckling behaviors of the stiff/soft bilayer are essentially determined by the parameters of the two films rather than by the compressive treatment [29, 31–37]. Buckling instability is an inherent property of bilayer films, and compressive strain triggers these buckling behaviors.

## 2. Influence of the Thickness Ratio on Buckling Instability in Stiff/Soft Bilayer Films

The thickness ratio directly determines how strongly the soft film constrains the bending deformation of the stiff membrane. For details, the soft film acts as an elastic support: a thick soft film can accommodate deformation locally, whereas a thinner soft film provides a stronger geometric constraint and may force the bilayer to deform over a larger length scale. Therefore, the thickness ratio often becomes a dominant parameter for determining the onset of wrinkling, the delay of period-doubling, and the competition between local surface wrinkling and global buckling.

Departing from previous studies that primarily focused on the "thick-soft substrate film limit," that is, a semi-infinite soft film, Auguste et al. address the relatively less explored yet significant scenario in flexible electronics and biological tissues where the soft film thickness is comparable to the stiff membrane thickness [38]. They systematically investigated the influence of the thickness ratio ($t_s/t_m$) on surface buckling instabilities and their subsequent evolution in elastic stiff/soft bilayer systems.

### 2.1. Influence of the thickness ratio on the critical strain for primary buckling instability

When the thickness of the soft film is significantly greater than that of the stiff membrane, the critical strain for the onset of buckling is primarily determined by the membrane-to-film modulus ratio [39]. Its value approaches the prediction of the classical thick-film theory. However, as the thickness ratio $t_s/t_m$ decreases (i.e., the soft film becomes progressively thinner), the onset of primary buckling is delayed, accompanied by a marked elevation in the critical strain. For example, when the modulus contrast is fixed at 50, finite element simulations show that as the thickness ratio $t_s/t_m$ decreases from approximately 10 to 2, the critical strain increases from about 0.05 to approximately 0.09 [39]. The underlying physical mechanism is that, as the soft film thickness decreases, the constraint imposed by the soft film on the stiff membrane's bending deformation is progressively enhanced, which restricts the bending degrees of freedom of the stiff membrane and thus increases the energetic cost required for buckling initiation. This result demonstrates that the thickness ratio not only influences the buckling wavelength and amplitude but also serves as an independent parameter capable of effectively tuning the onset conditions of buckling instability [40].

### 2.2. Influence of the thickness ratio on post-buckling evolution behavior

Compared to the primary buckling, the thickness ratio exerts a more pronounced influence on secondary instability and further evolution [38]. This effect can be observed from the experimental results shown in Figure 1. Here, the wrinkle aspect ratio, defined as the ratio of amplitude to wavelength, is used to quantify the development of the wrinkle morphology. At a small thickness contrast ($t_s/t_m = 3$, Figure 1(A)), wrinkles remain uniform and reach a high aspect ratio before period-doubling (secondary buckling instability) occurs, whereas at a larger thickness contrast ($t_s/t_m = 9$, Figure 1(B)), the wrinkle pattern enters the period-doubled state earlier and the achievable aspect ratio is reduced. Notably, the modulus contrast is fixed at 50.

**Figure 1**
**Confocal cross-sectional views of the evolution of wrinkles to period-doubling folds. A) The thickness ratio is 3. B) The thickness ratio is 9. $\varepsilon$ denotes the magnitude of the applied strain**

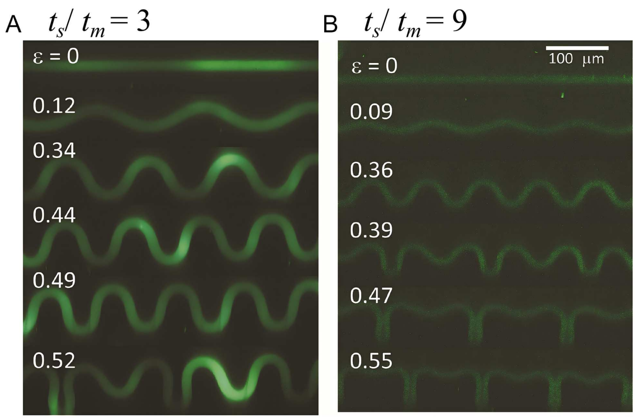


In conventional thick-film systems, periodic wrinkles typically undergo period-doubling folds at relatively low additional strains [41], thereby limiting the achievable wrinkle aspect ratio. Auguste et al. found that the critical strain for period-doubling instability reaches a maximum at $t_s/t_m = 3$ (Figure 2(A)), where the strong constraint imposed by the soft film significantly delays the onset of period-doubling. Figure 2(B) shows that at this thickness ratio, wrinkles can maintain periodicity and uniformity over a broad strain range, with their amplitude continuously increasing, allowing the wrinkle aspect ratio to reach up to approximately 0.6, which is significantly higher than in the thick-film scenario. In contrast, when the thickness ratio increases (e.g., $t_s/t_m \geq 9$), period-doubling occurs at relatively low strains, thereby limiting further amplification of the wrinkles. In fact, such period-doubling behavior has been reported in earlier studies. Brau et al., starting from nonlinear elasticity theory, interpreted period-doubling as a spatial bifurcation and attributed its origin to the interplay between nonlinearity and symmetry breaking in the system [24]. Auguste et al. further demonstrated that the geometric thickness ratio can serve as a key parameter for tuning the critical point of period-doubling instability, thereby offering a new degree of design freedom for controlling post-buckling evolution pathways [42].

Moreover, the study further indicates that when the thickness ratio is small and the modulus ratio is increased further, the system's evolution transitions from period-doubling folds to the formation of localized ridge structures [42]. This symmetry-breaking process enables the surface morphology to evolve from uniform wrinkles into periodic ridge structures, whose aspect ratio can further increase beyond 1. This indicates that the thickness ratio not only determines the critical strain for secondary instability but also governs the type of dominant post-buckling instability mode.

## 3. Global Buckling Deformation of the Stiff/Soft Bilayer Films

Under in-plane compression, the deformation instability of a stiff/soft bilayer manifests primarily as two distinct modes: local surface wrinkling and global buckling of the entire bilayer [43–48]. The competition between the bending stiffness of the stiff membrane and the elastic constraint provided by the soft film governs the selection of the instability mode (Table 1). Therefore, material parameters directly determine which form of instability emerges.

The elastic modulus represents a critical material parameter governing the instability mode selection in bilayer films, with its influence manifested primarily through the modulus ratio and the significant modulus mismatch between the stiff membrane and the soft film [49]. Poisson's ratio affects the buckling instability of bilayer films through the plane strain modulus, that is, $\overline{E_i} = E_i/(1-\mu_i^2)$. In bilayer films, Poisson's ratios of the soft film and stiff membrane are different. Poisson's ratio of the soft film is between 0.45 and 0.5, whereas that of the stiff membrane is between 0.2 and 0.35. By changing the effective modulus ratio, Poisson's ratio indirectly affects key instability parameters such as critical wavelength and critical strain [50].

### 3.1. Influence of the thickness ratio

When the thicknesses of the soft film and stiff membrane are similar, that is, the thickness ratio approaches 1, the instability mode of bilayer films favors global buckling deformation, which results from the dominant bending stiffness of the stiff membrane [51]. As the relative soft film thickness decreases, the bending stiffness of the stiff membrane dominates, local wrinkling

**Figure 2**

**Effect of thickness ratio on secondary buckling instability, that is, period-doubling fold. A) The critical strain for the onset of the period-doubling fold. The modulus contrast is fixed at 50. B) Wrinkle aspect ratio increases with applied strain, as shown here for a thickness ratio of 3.42**

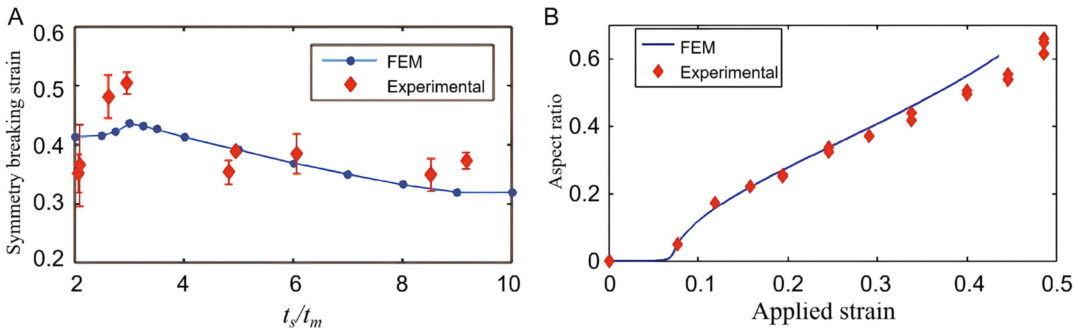


**Table 1**

**Comparisons between local surface wrinkling and global buckling in stiff/soft bilayer films**

| Feature | Local surface wrinkling | Global buckling |
|---|---|---|
| Deformation scope | Localized surface undulation | Uniform out-of-plane bending of the entire bilayer |
| Dominant mechanical factor | Stiff membrane bending stiffness vs. soft film elastic constraint | Bilayer film bending stiffness vs. applied in-plane compression |
| Role of soft film | Acts as an elastic foundation | Acts as a layered component of a bilayer film |
| Triggering geometric condition | w < wcr (or sufficiently thick substrate) | w > wcr (or sufficiently thin substrate) |

dominated by soft film deformation is suppressed, and the bilayer films undergo global buckling instability. When the soft film-to-stiff membrane thickness ratio decreases to a certain extent, the bending stiffness of the stiff membrane can no longer be offset by the elastic deformation of the film and becomes the main factor controlling structural deformation, promoting the occurrence of global buckling [28]. At this point, the bending behavior of the stiff membrane is no longer limited to local regions but manifests as uniform deformation of the entire layer. Meanwhile, the elastic constraint of the soft film fails, further promoting the formation of global buckling. In freestanding bilayer films, when the soft film thickness decreases to a level where sufficient elastic support cannot be provided, its constraint effect on the stiff membrane is significantly weakened, failing to limit the overall out-of-plane deformation of the stiff membrane and ultimately leading to global buckling [51]. Both relevant numerical simulations and experimental results show that when the soft film thickness decreases to a range comparable to the critical wavelength $\lambda_0$, the soft film can hardly absorb the compressive energy of the stiff membrane through its own deformation and loses its elastic constraint capacity, leading to the bending deformation of the entire bilayer film, that is, global buckling, rather than local periodic wrinkling [11].

### 3.2. The occurrence conditions of global deformation

There exists an explicit core geometric criterion for the occurrence of global buckling, namely, the relative relationship between the soft film thickness ($t_s$) and the critical width ($w_{cr}$) of the bilayer [52]. $w_{cr}$ is defined as the minimum width required for global buckling to occur; that is, when the bilayer width $w > w_{cr}$, global buckling will replace local wrinkling as the main instability mode. Ref. [52] provides an expression for $w_{cr}$ as shown below:

$$\begin{cases} w_{cr} = 4\pi(B)^{\frac{1}{2}}\left[\dfrac{\overline{E}_m^{\frac{2}{3}}}{(3\overline{E}_s)^{\frac{2}{3}}D} - \dfrac{0.3}{G_s(t_s+t_m)}\right]^{\frac{1}{2}}, \\ D = \overline{E}_s t_s + \overline{E}_m t_m \\ B = \dfrac{(\overline{E}_m t_m^2 - \overline{E}_s t_s^2)^2 + 4(\overline{E}_m \overline{E}_s)(t_m t_s)(t_m+t_s)^2}{12D} \end{cases} \tag{3}$$

where $t_s$ and $t_m$ are the thicknesses of the soft film and stiff membrane, respectively; $\overline{E}_s$ and $\overline{E}_m$ are the plane strain moduli of the soft film and the stiff membrane, respectively; $G_s$ is the shear modulus of the soft film; $D$ and $B$ are the effective axial rigidity and the effective bending rigidity of the whole bilayer film, respectively. We can find that the magnitude of $w_{cr}$ is directly influenced by the following parameters: the moduli, thicknesses, and Poisson's ratios of the two films, and cross-sectional stiffness characteristics among the geometric parameters.

Material parameters influence the onset of global buckling indirectly by modifying the critical geometric criteria. According to force-balance models, increasing the modulus ratio reduces the critical strain for local wrinkling, meaning local wrinkling occurs more readily [38]. At the same time, a larger modulus mismatch between the stiff membrane and the soft film reduces the critical width ($w_{cr}$), making the condition $w > w_{cr}$ more readily satisfied and thus promoting the occurrence of global buckling. Poisson's ratio indirectly adjusts the modulus ratio and geometric parameters, such as critical width and critical thickness, by changing the plane strain modulus. Different combinations of Poisson's ratios lead to differences in the critical strain for global buckling under the same geometric conditions, further expanding the regulatory space for the occurrence conditions of global buckling [53].

## 4. Scaling Law of the Buckling Evolution in the Stiff/Soft Bilayer Films

If the soft film in a stiff/soft bilayer system is sufficiently thick, the wrinkles will merge in pairs to form a period-doubling fold under continuous compression. In this mode, the surface perimeter of the fold $\lambda$ is $2\lambda_0$, corresponding to the second-order instability; this is subsequently followed by transitions into higher-order modes characterized by $\lambda = 4\lambda_0$, $8\lambda_0$, $16\lambda_0$, and so on. The order of instability can be quantified by the ratio of the surface perimeter of the buckling structure to $\lambda_0$. If the surface perimeter of a specific buckling mode equals $n\lambda_0$, the instability order is designated as $n = \lambda/\lambda_0$. As deformation increases, the evolution of buckling morphology (wrinkle, fold, and crease) and buckling mode ($n$-th order buckling structure) in stiff/soft bilayer systems is often coupled, resulting in more complex and diverse buckling behaviors. Despite extensive experimental and theoretical studies, a unified understanding and description remain lacking [28].

In fact, a detailed study of buckling behavior requires controlled and precise strain loading, which is difficult to achieve using traditional strain loading methods. To this end, Meng et al. propose a strategy involving perpendicular peeling of the bilayer films from a rigid substrate [9], as shown in Figure 3(A). This approach enables the controllable fabrication of large-area arrays of buckling structures, thereby demonstrating a novel pathway for micro/nano-fabrication (Figure 3(B)). Peeling and bending the soft film at a 90° angle induces compressive strain on the inner surface of the bend. The size of the compressed region is approximately on the order of several times the soft film's thickness, while the maximum compressive strain is inversely proportional to the film thickness. Consequently, this peeling strategy can ingeniously and precisely load large strains on soft films or stiff/soft bilayer systems, effectively addressing the challenge of achieving uniform, large-deformation buckling over large areas.

Meng et al. further demonstrated that, in a stiff/soft bilayer film, the most common buckling evolution initiates with wrinkles, transitions through folds, and terminates at creases. The crease is generally regarded as the final buckling mode, and its order is the final instability order $n$, which is primarily determined by the equivalent thickness ratio $t$ of the soft film and stiff membrane under routine experimental conditions, including room temperature and ambient humidity [9, 15]. Here, $t$ denotes the equivalent thickness ratio of the soft film to the stiff membrane, given by $t = (t_s/t_m)\,A^{-2}$, and $A = \pi\left(\frac{2}{3}\frac{\overline{E}_m}{\overline{E}_s}\right)^{1/3}\left[\frac{3-4\mu_s}{(1-\mu_s)^2}\right]^{1/3}$(see Eq. 1). For details, the final instability order $n$ is primarily determined by the equivalent thickness ratio $t = (t_s/t_m)\,A^{-2}$, exhibiting the stepwise dependence illustrated in Figure 4(A), which is the scaling law of the post-buckling instability in the stiff/soft bilayer. In fact, Figure 4(A) covers experimental results (stretch/compression, peel/bend), finite element simulations (covering various materials and thickness ratios), and literature data; that is, the universality of the scaling law was demonstrated by Meng et al. as rigorously as possible. Here, $t_1$ and $t_2$ denote the critical values of $t$ governing the transition of the final instability order between 1 and 2 and between 2 and 4, respectively. "peel" indicates data from peeling experiments, where compressive stress is applied by

**Figure 3**
**Precise control of large buckling deformation in stiff/soft bilayer via 90° peeling treatment. A) Schematic illustration of the 90° peeling process for a stiff/soft bilayer film from a rigid substrate, along with Scanning Electron Microscopy (SEM) characterization of the buckling structures in the bent region. B) SEM images. Upper overview images: the buckling morphologies in the bent region of SiO1.8/PDMS bilayer films with constant stiff membrane thickness ($t_m$) but varying soft film thicknesses ($t_s$). Insets at the bottom: the magnified views of three types of crease patterns**

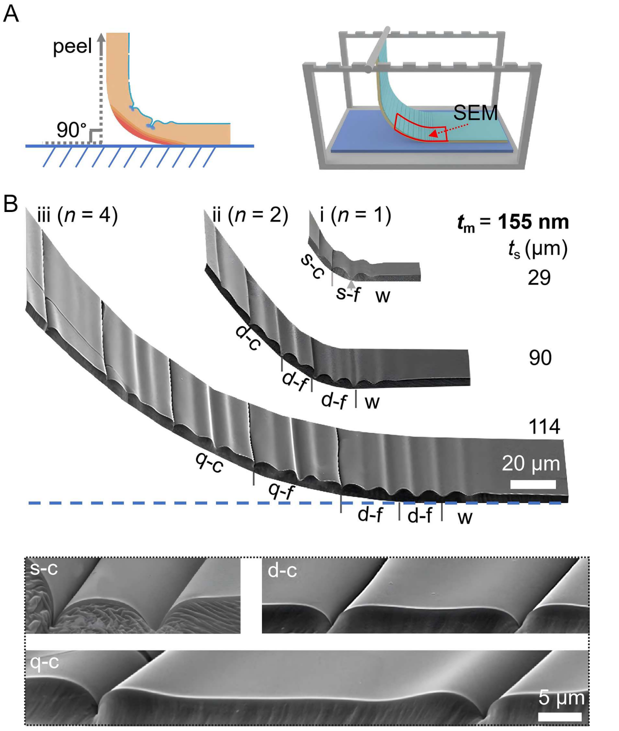


bending the stiff/soft bilayer at a 90° angle. “stretch” indicates data from stretching experiments, where compressive stress is applied via horizontal stretching of the bilayer. “Ref” indicates the experimental data collected in other references. SiO1.8, poly(methyl methacrylate) (PMMA), and Au represent three different stiff membranes, while PDMS serves as the soft film15.

As the equivalent thickness ratio $t$ increases from 0 but remains below the first critical value $t_1$, the buckling evolution exhibits only first-order instability, resulting in a final instability order of 1, as shown in Figure 4(B). Here, $t_1$ denotes the critical value of $t$ governing the transition of the final instability order between 1 and 2. Specifically, the morphology evolves from wrinkle to fold and then to crease, yet the surface perimeter remains constant. Consequently, the surface perimeter of all buckling structures is invariably $\lambda = 1\lambda_0$. When the equivalent thickness ratio exceeds the first critical value but is less than the second critical value $t_2$, the buckling evolution undergoes first- and second-order instabilities in succession, resulting in a final instability order of 2 (Figure 4(B)). Here, $t_2$ denotes the critical value of $t$ governing the transition of the final instability order between 2 and 4. Specifically, the morphology evolves from wrinkles to period-doubling folds and subsequently to period-doubling creases. In summary, if the equivalent thickness ratio falls between two critical values, the final instability order remains constant.

**Figure 4**
**Scaling law of the buckling evolution. A) The stepwise dependence of the final instability order n on the equivalent thickness contrast *t* in the stiff/soft bilayer films. B) Schematic illustration of the transition process among buckling modes at final instability orders of 1, 2, and 4**

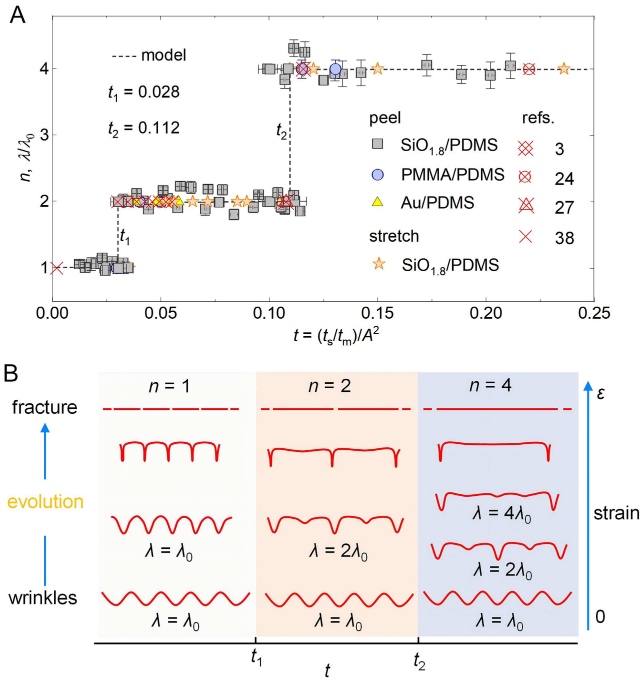


However, if the ratio crosses a critical threshold, the final instability order increases or decreases by one order. This constitutes the scaling law of post-buckling evolution.

According to this scaling law, by selecting stiff/soft bilayer films with a specific thickness ratio, we can obtain buckling patterns with predetermined morphologies and mode orders. In other words, the morphology and periodicity of the buckling structures can be custom-designed. Furthermore, an instability evolution map can be constructed based on the scaling law for all buckling structures of stiff/soft bilayer films, except ridge structures (Figure 4(B)). It should be noted that this scaling law is supported under the material systems and experimental conditions reported in the cited studies, and that additional data from broader systems would be needed to further establish its universality.

According to the scaling law, the soft film’s geometric thickness remains dominant even when it exceeds the stiff membrane thickness by several orders of magnitude. The significant role played by the soft film’s thickness is counterintuitive. It poses multi-scale challenges for both numerical simulations and theoretical analyses of buckling. Furthermore, in both natural systems and micro/nano-fabrication, strain is neither unidirectional nor homogeneous. For instance, stress-driven growth in biological systems, active morphogenesis, and thin-film self-organization all generate diverse and intricate wrinkle patterns within complex stress fields [54, 55]. The analytical understanding, predictable design, and application of such systems hold significant scientific promise. Therefore, establishing a post-buckling theory of stiff/soft bilayer films in accordance with the scaling law is of great significance yet remarkably challenging.

## 5. Applications of Buckling Behavior Controlled by Material Parameters

Traditionally, thin-film cutting is primarily achieved through ion etching. However, this etching process is time-consuming and relatively inefficient, and its essence involves ion implantation, which introduces significant ion contamination—especially in micrometer-scale or nanoscale films and particularly in single-atom-layer materials. For cutting thin films such as two-dimensional materials, there is an urgent need to develop efficient and clean new strategies [56]. It is easy to create fractures in stiff nanomembranes, but most fractures initiate at randomly distributed defects and propagate along uncontrolled paths; such cracks often become new defects that hinder the applications of the membranes [57]. Therefore, achieving fracture control in stiff thin films, especially nanomembranes such as two-dimensional materials, is highly desirable [58].

Meng et al. report a strategy for controlling nanomembrane fracture that relies on large buckling deformations. First, the stiff nanomembrane is transferred onto a soft film to form a stiff/soft bilayer (Figure 5(A)). Then, simply peeling the bilayer from the original substrate at a 90° bending angle can produce parallel, equally spaced fractures in the stiff membrane. The fracture period linearly depends on the thickness of the nanomembrane, enabling periodic initiation and strictly straight propagation of fractures in the nanomembrane. The reason for the above fracture behavior is that 90° bending induces a large compressive strain on the upper surface of the stiff/soft bilayer in the bending region, which further leads to buckling deformation on the surface. Because the compressive strain is sufficiently large, the buckling deformation evolves continuously from linear wrinkles to nonlinear creases with large deformations. The bottom of the crease experiences severe bending and compression of the nanomembrane, ultimately causing the stiff membrane to fracture along the central line at the bottom of the crease, as shown in Figure 5(B). As the creases are periodic, the fractures are also periodic, with a period equal to the surface perimeter of the crease. The surface perimeter of the crease is equal to $n$ times the critical wavelength $\lambda_0$. More complex patterns can be easily prepared in bilayer films depending on this periodic fracture behavior. Figure 5(C) shows two kinds of rhombic micro-flakes that are fabricated by twice peeling the bilayer along two selected directions. Meanwhile, we can create periodic nanoribbons or folding marks in the Au film and PMMA film by depositing them onto a thin PDMS film and applying a 90° peeling treatment [59], as shown in Figure 5(D). The thicknesses of the PMMA, Au membrane, and PDMS film are 3.2 μm, 310 nm, and 70 μm, respectively.

This fracture behavior is universal in stiff/soft bilayer systems and is thus capable of tailoring various stiff membranes into desired shapes and sizes, which can facilitate investigations of novel properties that depend on clean and regular edges and further allow these membranes to be applied in functional devices. This mechanical tailoring method will be complementary to previous fabrication methods based on ion etching and chemical processing, holding significant potential applications in the field of nano-fabrication.

A peeling angle equal to or slightly larger than 90° is crucial for effectively stimulating the above buckling pattern and corresponding fracture behavior [59]. If the peeling angle is less than 90° (Figure 6(a)), only wrinkles appear around the peeled front

**Figure 5**

**Fracture behavior of bilayer films under perpendicular peeling. A) Top panel: schematic illustration of in situ SEM imaging under peeling. Lower panel: side views of SEM images of buckling structures in $SiO_{1.8}$/PDMS bilayers with $t_m$ = 155 nm and $t_s$ = 112 um; serial numbers (i)–(iii) represent three milling locations of focused ion beams for characterizing cross-sections of creases in bending films. B) Images of focused ion beams (FIB) taken at the locations (i)–(iii), illustrating the fracture process at the bottom of a crease. C) SEM images of complex patterns in $SiO_{1.8}$/PDMS bilayer films. D) Confocal laser microscopy images of periodic fracture patterns or compressive marks in bilayer films with different stiff films and the same PDMS soft film**

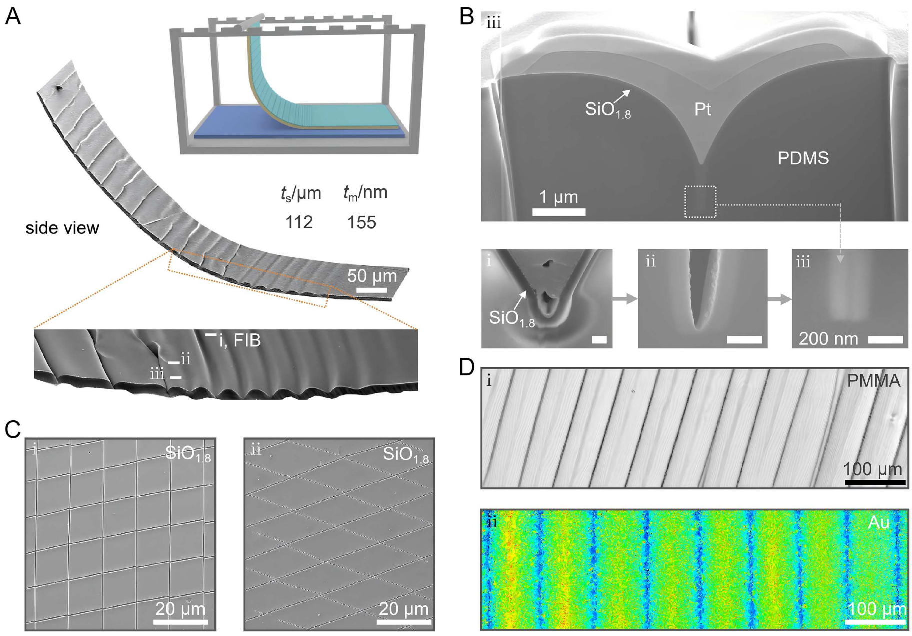

**Figure 6**
**Arbitrary fractures in $SiO_{1.8}$/PDMS bilayer stimulated by peeling treatment with a bending angle less than 90°. A) Schematic illustration of the peeling treatment. B) SEM image of a gradually changed wrinkle pattern in the vicinity of the peeled front, marked with a black arrow. C) SEM image of randomly distributed cracks in the peeled region**

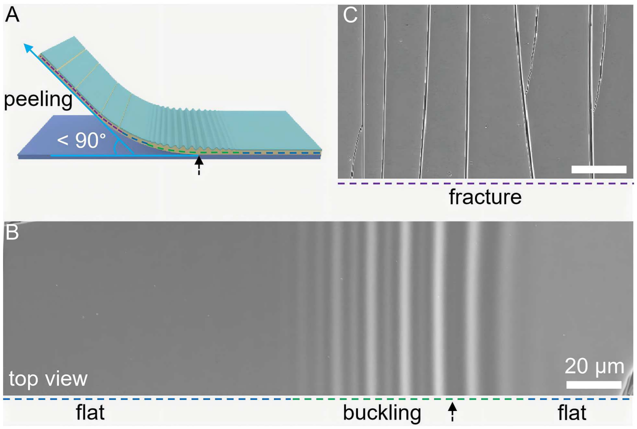


(Figure 6(b)), because the bending-induced compression does not suffice to trigger the wrinkle-to-crease transitions. Meanwhile, arbitrary fractures will appear in the peeled region away from the bending region due to the in-plane stretch applied for peeling (Figure 6(c)). This result indicates that the constraint of a 90° peeling angle acts as a geometric tool for creating the crease pattern and directing the fracture behavior of the stiff membrane on the soft film.

In fact, buckling behavior has numerous established applications, such as constructing flexible gratings based on periodic buckling arrays to modulate light transmission for smart windows, deducing bilayer film thickness and modulus from the relationship between buckling periodicity and material parameters [60], and fabricating flexible devices using buckling structures [3]—all of which are relatively conventional and straightforward. However, the fracture behavior of thin films, which follows from the scaling laws of buckling instability in bilayer films, directly demonstrates how material parameters selectively influence buckling instability. This is highly relevant to our theme, “The role of material parameters in the buckling behavior of stiff/soft bilayer films,” and therefore, we chose to emphasize it in the applications section of this review.

## 6. Conclusion

This work summarizes recent progress in understanding how material parameters control the buckling behavior of stiff/soft bilayer films. The main findings can be summarized as follows. First, the thickness ratio between the soft film and stiff membrane plays a dominant role in many finite-thickness bilayer systems. It affects not only the onset of primary wrinkling but also the development of secondary instability, including the transition from wrinkles to period-doubling folds. Second, the modulus ratio and Poisson’s ratio influence buckling behavior through the effective plane-strain modulus contrast. These parameters affect the critical wavelength, critical strain, and the competition between local surface wrinkling and global buckling. Third, the equivalent thickness ratio $t = (t_s/t_m)A^{-2}$ provides a useful scaling parameter for describing post-buckling evolution under routine experimental conditions, including room temperature and ambient humidity. It correlates with the final instability order and helps construct an instability evolution map for finite-thickness stiff/soft bilayer films.

Although extensive experimental results support this scaling description, existing analytical theories still mainly focus on first-order buckling or post-buckling behavior under the semi-infinite soft film approximation. Clearly, there is an urgent need to develop a post-buckling theory applicable to freestanding and finite-thickness stiff/soft bilayer films. This is, of course, highly challenging. Fortunately, a wealth of experimental results will serve as effective guidance. Meanwhile, a series of studies on the first-order buckling behavior of finite-thickness stiff/soft bilayer films have already been conducted by drawing on the perturbation analysis of Stokes flows [60–63]. Further research in this direction may offer valuable support for the development of post-buckling theory for such bilayer systems.

## Funding Support

This work was supported by the Natural Science Foundation of Jiangsu Province (BK20210271), the National Natural Science Foundation of China (12202189), and the Fellowship of the China National Postdoctoral Program for Innovative Talents (BX20200166).

## Ethical Statement

This study does not contain any studies with human or animal subjects performed by any of the authors.

## Conflicts of Interest

The authors declare that they have no conflicts of interest to this work.

## Data Availability Statement

Data are available from the corresponding author upon reasonable request.

## Author Contribution Statement

**Hui He:** Conceptualization, Formal analysis, Investigation, Writing – original draft. **Yufeng Chen:** Methodology, Validation, Formal analysis, Investigation, Data curation, Writing – original draft, Writing – review & editing. **Xintong Shen:** Methodology, Validation, Formal analysis, Investigation, Data curation, Writing – original draft, Writing – review & editing. **Feng Chen:** Resources, Data curation. **Zhixiang Wang:** Resources, Data curation. **Yancheng Meng:** Conceptualization, Methodology, Validation, Investigation, Data curation, Writing – original draft, Writing – review & editing, Supervision, Project administration, Funding acquisition.

## References

[1] Bowden, N., Brittain, S., Evans, A. G., Hutchinson, J. W., & Whitesides, G. M. (1998). Spontaneous formation of ordered structures in thin films of metals supported on an elastomeric polymer. *Nature*, *393*(6681), 146–149. https://doi.org/10.1038/30193

[2] Shiba, K., Saito, K., Minami, K., Arai, S., Yoshikawa, G., Sun, L., & Tenjimbayashi, M. (2024). Syneresis-driven self-refilling printing of geometry/component-controlled nano/microstructures. *Advanced Science*, *11*(40), 2405151. https://doi.org/10.1002/advs.202405151

[3] Pocivavsek, L., Dellsy, R., Kern, A., Johnson, S., Lin, B., Lee, K. Y. C., & Cerda, E. (2008). Stress and fold localization in thin elastic membranes. *Science*, *320*(5878), 912–916. https://doi.org/10.1126/science.1154069

[4] Hutchinson, J. W. (2013). The role of nonlinear substrate elasticity in the wrinkling of thin films. *Philosophical Transactions of the Royal Society A: Mathematical, Physical and Engineering Sciences*, *371*(1993), 20120422. https://doi.org/10.1098/rsta.2012.0422

[5] Wang, C. G., Liu, Y. P., & Tan, H. F. (2016). Global and local interactive buckling behavior of a stiff film/compliant substrate system. *International Journal of Solids and Structures*, *102*, 176–185. https://doi.org/10.1016/j.ijsolstr.2016.10.006

[6] Zhong, S., Zhu, Z., Huo, Q., Long, Y., Gong, L., Ma, Z., . . . , & Chen, X. (2024). Designed wrinkles for optical encryption and flexible integrated circuit carrier board. *Nature Communications*, *15*(1), 5616. https://doi.org/10.1038/s41467-024-50069-7

[7] Son, S. Y., Lee, G., Wang, H., Samson, S., Wei, Q., Zhu, Y., & You, W. (2022). Integrating charge mobility, stability and stretchability within conjugated polymer films for stretchable multifunctional sensors. *Nature Communications*, *13*(1), 2739. https://doi.org/10.1038/s41467-022-30361-0

[8] Zhang, S., Wu, J., Hou, Z.-L., Hu, P., Cai, B., Liang, C., . . . , & Wang, G.-S. (2026). Regular-wrinkling tunable MXene lattice for electromagnetic interference shielding. *Nature Communications*, *17*, 1275. https://doi.org/10.1038/s41467-025-68035-2

[9] Yang, Q., Yang, J., Hu, Y., Niu, X., Liu, Z., Zou, J., . . . , & Deng, X. (2025). A skin-inspired durable de-icing surface with boosting interfacial cracks. *National Science Review*, *12*(3), nwaf005. https://doi.org/10.1093/nsr/nwaf005

[10] Junisu, B. A., Chang, I. C. Y., Lin, C. C., & Sun, Y. S. (2022). Surface wrinkling on polymer films. *Langmuir*, *38*(12), 3907–3916. https://doi.org/10.1021/acs.langmuir.2c00156

[11] Nikravesh, S., Ryu, D., & Shen, Y. L. (2020). Instabilities of thin films on a compliant substrate: Direct numerical simulations from surface wrinkling to global buckling. *Scientific Reports*, *10*(1), 5728. https://doi.org/10.1038/s41598-020-62600-z

[12] Li, S., Sha, Y., Wu, Y., Gao, Y., He, M., Wang, X., . . . , & Mai, X. (2025). Experimental investigation of indoor lighting/thermal characteristics of highly sensitive mechanochromic energy-saving windows. *Energy*, *322*, 135659. https://doi.org/10.1016/j.energy.2025.135659

[13] Humenik, M., Zhou, Z., Kopsch, F., Knapp, A., Yu, Z., Schlicke, H., . . . , & Fery, A. (2026). Wrinkling-based patterning and recombinant spider silk-based coating technologies-toward novel applications. *Small*, *22*(3), e08468. https://doi.org/10.1002/smll.202508468

[14] Zhao, Y., Yang, X., Cheng, Z., Lau, C. H., Ma, J., & Shao, L. (2023). Surface manipulation for prevention of migratory viscous crude oil fouling in superhydrophilic membranes. *Nature Communications*, *14*(1), 2679. https://doi.org/10.1038/s41467-023-38419-3

[15] Trindade, A. C. (2024). Controlled surface textures of elastomeric polyurethane Janus particles: A comprehensive review. *Polymers*, *16*(13), 1835. https://doi.org/10.3390/polym16131835

[16] Suñé, M., Arratia, C., Bonfils, A. F., Vella, D., & Wettlaufer, J. S. (2023). Wrinkling composite sheets. *Soft Matter*, *19*(45), 8729–8743. https://doi.org/10.1039/d3sm00430a

[17] Meng, Y., He, H., Liu, X., Zhang, J., Chen, F., Chen, Y., . . . , & Guo, W. (2026). Universal expression for the intrinsic periodic length at the threshold of the primary buckling instability in finite-thickness stiff/soft bilayer films. *Acta Mechanica Sinica*, *42*(1), 451229. https://doi.org/10.1007/s10409-026-51229-x

[18] Guan, X., Sarma, A. P., Hamesh, E. K., Yang, J., Nguyen, N., Cerda, E., . . . , & Velankar, S. S. (2022). Compression-induced buckling of thin films bonded to viscous substrates: Uniform wrinkles vs localized ridges. *International Journal of Solids and Structures*, *254*, 111843. https://doi.org/10.1016/j.ijsolstr.2022.111843

[19] Lampart, F. L., Vetter, R., Yamauchi, K. A., Wang, Y., Runser, S., Strohmeyer, N., . . . , & Iber, D. (2025). Morphometry and mechanical instability at the onset of epithelial bladder cancer. *Nature Physics*, *21*(2), 279–288. https://doi.org/10.1038/s41567-024-02735-2

[20] Mane, S., & Huang, R. (2022). Rate-dependent wrinkling and subsequent bifurcations of an elastic thin film on a viscoelastic layer. *International Journal of Solids and Structures*, *257*, 111592. https://doi.org/10.1016/j.ijsolstr.2022.111592

[21] Klopp, C., Trittel, T., Harth, K., & Stannarius, R. (2021). Smectic free-standing films under fast lateral compression. *Soft Matter*, *18*(1), 146–155. https://doi.org/10.1039/d1sm01207j

[22] Yang, K., Zhou, Y., Ling, Y., Tsia, K. K., Zeng, H., & Wong, K. K. (2024). Spectral period doubling and encoding of dissipative optical solitons via gain control. *PhotoniX*, *5*(1), 26. https://doi.org/10.1186/s43074-024-00141-8

[23] Wang, J., & Dortdivanlioglu, B. (2025). Size-dependent instabilities in highly deformable strain-gradient materials. *Journal of the Mechanics and Physics of Solids*, *205*, 106307. https://doi.org/10.1016/j.jmps.2025.106307

[24] Brau, F., Vandeparre, H., Sabbah, A., Poulard, C., Boudaoud, A., & Damman, P. (2011). Multiple-length-scale elastic instability mimics parametric resonance of nonlinear oscillators. *Nature Physics*, *7*(1), 56–60. https://doi.org/10.1038/nphys1806

[25] Xin, M., & Davidovitch, B. (2021). Stretching Hookean ribbons part II: From buckling instability to far-from-threshold wrinkle pattern. *The European Physical Journal E*, *44*(7), 94. https://doi.org/10.1140/epje/s10189-021-00088-9

[26] Nikravesh, S., & Shen, Y. L. (2024). Wrinkle, fold, and ridge patterns of thin films attached to a compliant substrate: Direct numerical simulations involving plastic yielding. *Thin-Walled Structures*, *198*, 111649. https://doi.org/10.1016/j.tws.2024.111649

[27] Wang, Q., & Zhao, X. (2015). A three-dimensional phase diagram of growth-induced surface instabilities. *Scientific Reports*, *5*(1), 8887. https://doi.org/10.1038/srep08887

[28] Zhao, R., Zhang, T., Diab, M., Gao, H., & Kim, K. S. (2015). The primary bilayer ruga-phase diagram I: Localizations in ruga evolution. *Extreme Mechanics Letters*, *4*, 76–82. https://doi.org/10.1016/j.eml.2015.04.006

[29] Meng, Y., Xiang, H., Zhang, J., Yin, J., Li, L., Zhang, Z., & Guo, W. (2023). The universal scaling law for wrinkle evolution in stiff membranes on soft films. *Matter*, *6*(6), 1964–1974. https://doi.org/10.1016/j.matt.2023.03.030

[30] Zhao, R., Diab, M., & Kim, K. S. (2016). The primary bilayer ruga-phase diagram II: Irreversibility in ruga evolution. *Journal of Applied Mechanics*, *83*(9), 091004. https://doi.org/10.1115/1.4033722
[31] Park, J. H., Holló, G., & Schaerli, Y. (2024). From resonance to chaos by modulating spatiotemporal patterns through a synthetic optogenetic oscillator. *Nature Communications*, *15*(1), 7284. https://doi.org/10.1038/s41467-024-51626-w
[32] Shang, H., Dong, H., Wu, Y., Deng, F., Liang, X., Hu, S., & Shen, S. (2024). Mechanical control of polar patterns in wrinkled thin films via flexoelectricity. *Physical Review Letters*, *132*(11), 116201. https://doi.org/10.1103/PhysRevLett.132.116201
[33] Guo, Y., & Nie, G. (2024). Theoretical and numerical analysis of period-doubling bifurcation in sandwich systems. *International Journal of Solids and Structures*, *294*, 112744. https://doi.org/10.1016/j.ijsolstr.2024.112744
[34] Zhao, Y., & Fang, F. (2024). Bio-inspired hierarchical wrinkles for tunable infrared reflectance. *Surfaces and Interfaces*, *45*, 103832. https://doi.org/10.1016/j.surfin.2023.103832
[35] Fu, Y., Wang, Y. S., & Fu, Y. (2024). Wrinkling of a film/substrate bilayer with periodic material properties: An assessment of the Winkler foundation model. *International Journal of Non-Linear Mechanics*, *166*, 104815. https://doi.org/10.1016/j.ijnonlinmec.2024.104815
[36] Kumar, A., & Audoly, B. (2025). Wavelength selection in the twist buckling of pre-strained elastic ribbons. *Journal of the Mechanics and Physics of Solids*, *196*, 106005. https://doi.org/10.1016/j.jmps.2024.106005
[37] Airoldi, C. A., Chen, C., Herrera-Ubaldo, H., Fu, H., Lugo, C. A., Ponraj, U., . . . , & Glover, B. J. (2025). Characterisation of cuticle mechanical properties: Analysing stiffness in layered living systems to understand surface buckling patterns. *Soft Matter*, *21*(42), 8231–8241. https://doi.org/10.1039/d4sm01406e
[38] Auguste, A., Yang, J., Jin, L., Chen, D., Suo, Z., & Hayward, R. C. (2018). Formation of high aspect ratio wrinkles and ridges on elastic bilayers with small thickness contrast. *Soft Matter*, *14*(42), 8545–8551. https://doi.org/10.1039/c8sm01345d
[39] Zang, J., Zhao, X., Cao, Y., & Hutchinson, J. W. (2012). Localized ridge wrinkling of stiff films on compliant substrates. *Journal of the Mechanics and Physics of Solids*, *60*(7), 1265–1279. https://doi.org/10.1016/j.jmps.2012.03.009
[40] Wang, X., Wang, S., & Holland, M. A. (2024). Axonal tension contributes to consistent fold placement. *Soft Matter*, *20*(14), 3053–3065. https://doi.org/10.1039/d4sm00129j
[41] Auguste, A., Jin, L., Suo, Z., & Hayward, R. C. (2014). The role of substrate pre-stretch in post-wrinkling bifurcations. *Soft Matter*, *10*(34), 6520–6529. https://doi.org/10.1039/c4sm01038h
[42] Jin, L., Auguste, A., Hayward, R. C., & Suo, Z. (2015). Bifurcation diagrams for the formation of wrinkles or creases in soft bilayers. *Journal of Applied Mechanics*, *82*(6), 061008. https://doi.org/10.1115/1.4030384
[43] Ma, S., & Chen, M. (2025). Stability conditions of tensegrity structures considering local and global buckling. *International Journal of Mechanical Sciences*, *287*, 109951. https://doi.org/10.1016/j.ijmecsci.2025.109951
[44] Liu, J., Zhang, S., He, J., Wen, G., Xie, Y. M., & Wiercigroch, M. (2026). Origami-inspired acoustic metamaterials: Real-time tunable bandgap and sound attenuation. *International Journal of Mechanical Sciences*, *314*, 111391. https://doi.org/10.1016/j.ijmecsci.2026.111391
[45] Liang, M., Wang, X., Correia, J. R., Ding, J., Zhou, J., & Wu, Z. (2025). Local and global buckling behaviors of pultruded fiber-reinforced polymer box columns with multi-directional fiber layups under axial compression. *Composites Part B: Engineering*, *297*, 112265. https://doi.org/10.1016/j.compositesb.2025.12265
[46] Kwak, H., Lee, J., Kim, J., Jo, H., Ki, K., & Lee, A. (2026). Wrinkling of thin films in pre-stretched soft substrate trilayers. *International Journal of Mechanical Sciences*, *312*, 111213. https://doi.org/10.1016/j.ijmecsci.2026.111213
[47] Jeleniewicz, K., & Piekarczuk, A. (2026). Experimental and numerical methodology for assessing the bending behaviour of thin-walled steel angle members: A representative case study. *Applied Sciences*, *16*(5), 2220. https://doi.org/10.3390/app16052220
[48] Hou, Y., Wen, C., Liu, K., Duan, J., Sun, H., & Guo, Y. (2025). Local and global buckling prevention design of transformed triangular corrugated plates under shear and bending. *Thin-Walled Structures*, *211*, 113135. https://doi.org/10.1016/j.tws.2025.113135
[49] Ebata, Y., Croll, A. B., & Crosby, A. J. (2012). Wrinkling and strain localizations in polymer thin films. *Soft Matter*, *8*(35), 9086–9091. https://doi.org/10.1039/C2SM25859E
[50] Bush, K. A., Rolston, N., Gold-Parker, A., Manzoor, S., Hausele, J., Yu, Z. J., . . . , & McGehee, M. D. (2018). Controlling thin-film stress and wrinkling during perovskite film formation. *ACS Energy Letters*, *3*(6), 1225–1232. https://doi.org/10.1021/acsenergylett.8b00544
[51] Takei, A., Jin, L., Fujita, H., Takei, A., Fujita, H., & Jin, L. (2016). High-aspect-ratio ridge structures induced by plastic deformation as a novel microfabrication technique. *ACS Applied Materials & Interfaces*, *8*(36), 24230–24237. https://doi.org/10.1021/acsami.6b07957
[52] Nikravesh, S., Ryu, D., & Shen, Y. L. (2020). Instabilities of thin films on a compliant substrate: Direct numerical simulations from surface wrinkling to global buckling. *Scientific Reports*, *10*(1), 5728. https://doi.org/10.1038/s41598-020-62600-z
[53] Ram, S. K., Desta, D., Rizzoli, R., Falcao, B. P., Eriksen, E. H., Bellettato, M., & Balling, P. (2017). Efficient light-trapping with quasi-periodic uniaxial nanowrinkles for thin-film silicon solar cells. *Nano Energy*, *35*, 341–349. https://doi.org/10.1016/j.nanoen.2017.04.016
[54] Li, J., Arora, N., & Rudykh, S. (2021). Elastic instabilities, microstructure transformations, and pattern formations in soft materials. *Current Opinion in Solid State and Materials Science*, *25*(2), 100898. https://doi.org/10.1016/j.cossms.2021.100898
[55] Yang, S., Khare, K., & Lin, P. C. (2010). Harnessing surface wrinkle patterns in soft matter. *Advanced Functional Materials*, *20*(16), 2550–2564. https://doi.org/10.1002/adfm.201000034
[56] Shim, J., Bae, S. H., Kong, W., Lee, D., Qiao, K., Nezich, D., . . . , & Kim, J. (2018). Controlled crack propagation for atomic precision handling of wafer-scale two-dimensional materials. *Science*, *362*(6415), 665–670. https://doi.org/10.1126/science. aat9458
[57] Huang, L., Zheng, F., Deng, Q., Thi, Q. H., Wong, L. W., Cai, Y., . . . , & Zhao, J. (2020). Anomalous fracture in two-dimensional rhenium disulfide. *Science Advances*, *6*(47), eabc2282. https://doi.org/10.1126/sciadv.abc2282

[58] Yang, Y., Song, Z., Lu, G., Zhang, Q., Zhang, B., Ni, B., . . . , & Lou, J. (2021). Intrinsic toughening and stable crack propagation in hexagonal boron nitride. *Nature*, *594*(7861), 57–61. https://doi.org/10.1038/s41586-021-03448-2

[59] Meng, Y., Zhang, J., Li, B., Li, L., Wang, Q., & Guo, W. (2023). Periodic fracture behaviour of nanomembranes. *Materials Horizons*, *10*(8), 3135–3139. https://doi.org/10.1039/d3mh00422h

[60] Stafford, C. M., Harrison, C., Beers, K. L., Karim, A., Amis, E. J., VanLandingham, M. R., . . . , & Simonyi, E. E. (2004). A buckling-based metrology for measuring the elastic moduli of polymeric thin films. *Nature Materials*, *3*(8), 545–550. https://doi.org/10.1038/nmat1175

[61] Huang, R., & Suo, Z. (2002). Instability of a compressed elastic film on a viscous layer. *International Journal of Solids and Structures*, *39*(7), 1791–1802. https://doi.org/10.1016/S0020-7683(02)00011-2

[62] Sridhar, N., Srolovitz, D. J., & Suo, Z. (2001). Kinetics of buckling of a compressed film on a viscous substrate. *Applied Physics Letters*, *78*(17), 2482–2484. https://doi.org/10.1063/1.1368180

[63] Ball, T. V., & Balmforth, N. J. (2023). Viscous flow beneath a viscous or plastic skin. *Journal of Fluid Mechanics*, *957*, A9. https://doi.org/10.1017/jfm.2023.17

**How to Cite:** He, H., Chen, Y., Shen, X., Chen, F., Wang, Z., & Meng, Y. (2026). The Role of Material Parameters in the Buckling Behavior of Stiff/Soft Bilayer Films. *Smart Wearable Technology*. https://doi.org/10.47852/bonviewSWT62029149